THE JOURNAL OF PHYSICAL CHEMISTRY C

Article

pubs.acs.org/JPCC

Synthesis and Efficient Visible Light Photocatalytic Hydrogen Evolution of Polymeric g-C_3N_4 Coupled with CdS Quantum Dots

Lei Ge,[†,‡] Fan Zuo,[†] Jikai Liu,[†] Quan Ma,[†] Chen Wang,[†] Dezheng Sun,[†] Ludwig Bartels,[†] and Pingyun Feng*[,†]

[†]Department of Chemistry, University of California, Riverside, California 92521, United States

[‡]Department of Materials Science and Engineering, College of Science, China University of Petroleum Beijing, No. 18 Fuxue Rd., Beijing 102249, People's Republic of China

ABSTRACT: Novel CdS quantum dot (QD)-coupled graphitic carbon nitride (g-C_3N_4) photocatalysts were synthesized via a chemical impregnation method and characterized by X-ray diffraction, transmission electron microscopy, ultraviolet–visible diffuse reflection spectroscopy, X-ray photoelectron spectroscopy, Fourier transform infrared spectroscopy, and photoluminescence spectroscopy. The effect of CdS content on the rate of visible light photocatalytic hydrogen evolution was investigated for different CdS loadings using platinum as a cocatalyst in methanol aqueous solutions. The synergistic effect of g-C_3N_4 and CdS QDs leads to efficient separation of the photogenerated charge carriers and, consequently, enhances the visible light photocatalytic H_2 production activity of the materials. The optimal CdS QD content is determined to be 30 wt %, and the corresponding H_2 evolution rate was 17.27 μmol·h^{-1} under visible light irradiation, ~9 times that of pure g-C_3N_4. A possible photocatalytic mechanism of the CdS/g-C_3N_4 composite is proposed and corroborated by photoluminescence spectroscopy and photoelectrochemical curves.

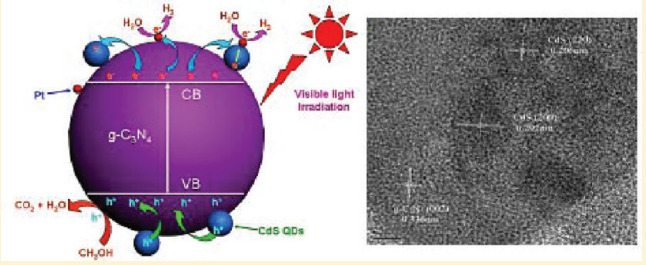

1. INTRODUCTION

Photocatalytic H_2 evolution from water over semiconductors by solar irradiation has received considerable attention due to its potential application in a hydrogen economy.[1−5] The creation of simple and efficient photocatalysts utilizing visible light (~43% of the solar spectrum) as opposed to by UV light (~4% of the solar spectrum) is of great importance for practical application.[6−11] H_2 production under visible light irradiation has been demonstrated with several semiconductor photocatalysts, including multicomponent oxides, sulfides, oxynitrides, and polymers.[12−17] Recently, polymeric graphitic carbon nitride (g-C_3N_4) has shown good photocatalytic performance for hydrogen and oxygen evolution from water in the visible light region.[18−20] Moreover, the precursors of g-C_3N_4 are inexpensive and the synthesis is comparatively simple, rendering g-C_3N_4 a promising candidate for photocatalytic water splitting.[21,22] However, the photocatalytic efficiency of pure g-C_3N_4 is limited by the high recombination rate of its photogenerated electron–hole pairs.[23] To enhance its photocatalytic performance, a number of methods have been exploited, including porous structures,[20] doping and coupling of g-C_3N_4 with metals,[24] graphene,[25,26] activated by protonation,[27] and organic dyes.[28]

Semiconductor QDs, such as CdS,[29] CdSe,[30] CdTe,[31] PbS,[32] and $CuInS_2$,[33] have been attached to photocatalysts to improve their photoactivity in the visible spectrum. Peng et al.[34] reported a CdS QD-sensitized TiO_2 photocatalyst with a hydrogen generation rate of 2200 μmol·h^{-1}·W^{-1} under visible light illumination. Gao et al[35] developed a CdS/TiO_2 heterojunction structure using CdS QDs as a sensitizer, thereby enhancing the photoactivity of TiO_2 nanotube photoelectrodes. Daskalaki et al[36] prepared Pt activated CdS/TiO_2 that produces H_2 at a high quantum efficiency from a simulated solar spectrum.

To the best of our knowledge, there are no reports on the synthesis and application of CdS QDs/g-C_3N_4 composites for hydrogen evolution via photocatalytic water splitting. In this study, we use chemical impregnation to combine CdS QDs and g-C_3N_4 and investigate the effect of the CdS QD content on the rate of photocatalytic hydrogen evolution in methanol aqueous solutions. This study may provide a new insight for the synthesis of photocatalysts with high visible light activities.

2. EXPERIMENTAL SECTION

2.1. Synthesis of the Photocatalyst. All chemicals were reagent grade and used without further purification. Metal-free g-C_3N_4 powder was synthesized by heating 2 g of cyanamide in an alumina combustion boat for 4 h under a nitrogen gas flow (10 mL/min) to 550 °C at a heating rate of 10 °C min^{-1}, followed by 4 h at that temperature prior to cooling. The product was collected and ground into powder.

Received: April 30, 2012
Revised: May 24, 2012
Published: May 29, 2012

CdS QDs were prepared in the aqueous phase with TGA (thioglycollic acid) as stabilizer by adding TGA to a 75 mM $Cd(NO_3)_2{\cdot}2H_2O$ solution with a mole ratio of 1:2 (TGA/CdS QDs) at a pH value of 10.5 adjusted by the addition of 1 mol/L sodium hydroxide solution (NaOH). After adding Na_2S, the mixture was stirred at 65 °C for 30 min and aged for another 90 min. Subsequently, the solution was centrifuged, and the QDs were extracted and rinsed with distilled water. The sample was redispersed in distilled water to obtain a CdS QDs solution.

CdS QDs/g-C_3N_4 composite photocatalysts were prepared as follows: Different amounts of solutions containing the CdS quantum dots were ultrasonicated for 30 min to completely disperse the CdS QDs. The as-prepared g-C_3N_4 powder (0.3 g) was added to the above solution and stirred for 24 h. After that, the product was collected by centrifugation, washed with distilled water, and dried in an oven at 70 °C for 24 h. Finally, the samples were heated to 300 °C for 1 h. Photocatalyst samples with weight percentages of CdS QDs of 0, 10, 20, 30, 40, and 50 wt % were prepared.

2.2. Characterization. The crystal structure of the samples was investigated using X-ray diffraction (XRD; Bruker D8 Advance X-ray diffractometer) with Cu Kα radiation at a scan rate of 0.1° 2θ s^{-1}. The acceleration voltage and the applied current were 40 kV and 40 mA, respectively. The morphology of the samples was examined by transmission electron microscopy (TEM; FEI JEM-2100 and FEI Tecnai G^2 F20) operated at 200 kV. UV−vis diffuse reflection spectroscopy (DRS) was performed on a Shimadzu UV-3100 spectrophotometer using $BaSO_4$ as the reference. X-ray photoelectron spectroscopy (XPS) measurements were done on a Scienta R3000 XPS instrument with a Mg Kα source. Infrared spectra were obtained on KBr pellets on an Equinox 55 spectrometer (Bruker) in the range of 4000−500 cm^{-1}. The photoluminescence (PL) spectra of the photocatalyst were obtained by a Varian Cary Eclipse spectrometer with an excitation wavelength of 325 nm.

2.3. Photocatalytic Activity. The photocatalytic H_2 evolution experiments were performed in a 300 mL quartz reactor at ambient temperature. The reactor was connected to a closed-cycle circulation system. The PLS-SXE 300UV Xe arc lamp with a UV cutoff filter (>400 nm) was used as the light source. In a typical photocatalytic experiment, 0.1 g of photocatalyst powder was suspended in 120 mL of aqueous solution containing 25% methanol by volume. The loading of 1.0 wt % Pt cocatalyst was conducted by directly dissolving H_2PtCl_6 into the suspension, followed by stirring and irradiation (300 W Xe arc lamp) for 30 min at room temperature to reduce the Pt species. Before photocatalytic experiments, the reaction vessel was evacuated for 30 min to remove dissolved oxygen and to ensure anaerobic conditions. The products were analyzed by gas chromatography (Shimadzu GC-8A, high-purity argon as a carrier gas) using a thermal conductivity detector.

2.4. Photoelectrochemical Measurements. Photocurrent measurements were performed on an electrochemical analyzer (Solartron Instruments SI 1287) in a standard three-electrode configuration with a Pt wire as the counter electrode and a Ag/AgCl (in saturated KCl) reference electrode. Irradiation proceeded by a Xe arc lamp through a UV cutoff filter (λ > 400 nm) at an intensity of 9.6 mW/cm^2. Na_2SO_4 (0.01M) aqueous solution was used as the electrolyte. The working electrodes were prepared as follows: 0.05 g of the ground sample was mixed with 1 mL of distilled water, and 0.1 mL of Liquion (Ion Power, Inc.) solution was added to make a slurry. A 2 cm × 0.5 cm ITO glass electrode was covered with this slurry and dried at 120 °C for 30 min.

3. RESULTS AND DISCUSSION

3.1. Characterization of CdS QDs/g-C_3N_4 Composite Samples. Figure 1 compares the XRD patterns of CdS/g-C_3N_4 samples of varying CdS QD contents (10−50 wt %) with patterns for pure g-C_3N_4 and CdS QDs. The XRD pattern recorded for pure g-C_3N_4 has two distinct diffraction peaks: the strong one at 27.40° represents the stacking of the conjugated double bonds, which is indexed for graphitic materials as the (002) peak and corresponds well to the interlayer *d*-spacing of g-C_3N_4 of 0.336 nm, and the weak diffraction peak at 13.04° corresponds to an interplanar separation of 0.672 nm and is indexed as (100) in JCPDS 87-1526. These two diffraction peaks are in good agreement with the g-C_3N_4 reported in the literature.[37,39] The XRD pattern of pure CdS QDs has four discernible diffraction peaks, which confirms the face-centered cubic structure of CdS according to JCPDS 89-0440. The CdS QDs/g-C_3N_4 composite samples exhibit diffraction peaks corresponding to both g-C_3N_4 and CdS, reflecting the presence of two phases.

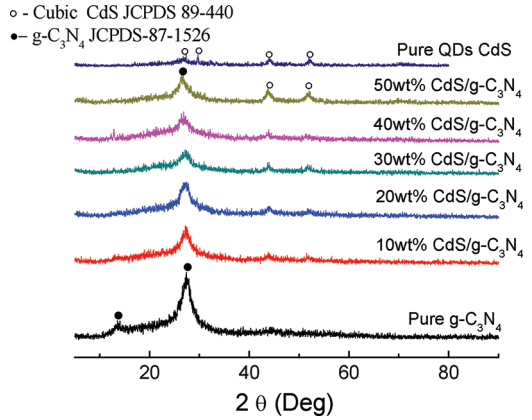

Figure 1. XRD patterns of pure g-C_3N_4, as well as of the CdS QDs/g-C_3N_4 composite photocatalysts.

The morphology and microstructure of the CdS QDs was investigated by TEM; as shown in Figure 2a, the CdS QDs have diameters of 2−5 nm and their crystallinity can be resolved (Figure 2b). The lattice spacings measured for the crystalline planes are 0.292 and 0.337 nm, corresponding to the (200) and (111) planes of fcc CdS (JCPDS 89-0440).[38] TEM images of QD CdS/g-C_3N_4 composite samples (Figure 3a) reveal sheetlike particles decorated with crystalline CdS QDs with different orientations, and the CdS QDs are distributed randomly on the g-C_3N_4 sheets (Figure 3b). By measuring the lattice parameters and comparing with the data in JCPDS, the lattice spacing of g-C_3N_4 crystallites is recognized as 0.336 nm, belonging to the (002) plane of hexagonal g-C_3N_4 (JCPDS 87-1526). The CdS QDs attached via their (200) and (220) crystal planes (lattice spacings of 0.292 and 0.206 nm, JCPDS 89-0440) to the g-C_3N_4.

The optical absorption of the as-prepared CdS QDs/g-C_3N_4 samples is shown in Figure 4. The pure g-C_3N_4 sample absorbs from the UV through the visible range up to 460 nm, which can be assigned to the intrinsic band gap of g-C_3N_4 (2.7 eV). The pure CdS QDs have absorption in the visible range with a band

dx.doi.org/10.1021/jp3041692 | J. Phys. Chem. C 2012, 116, 13708−13714

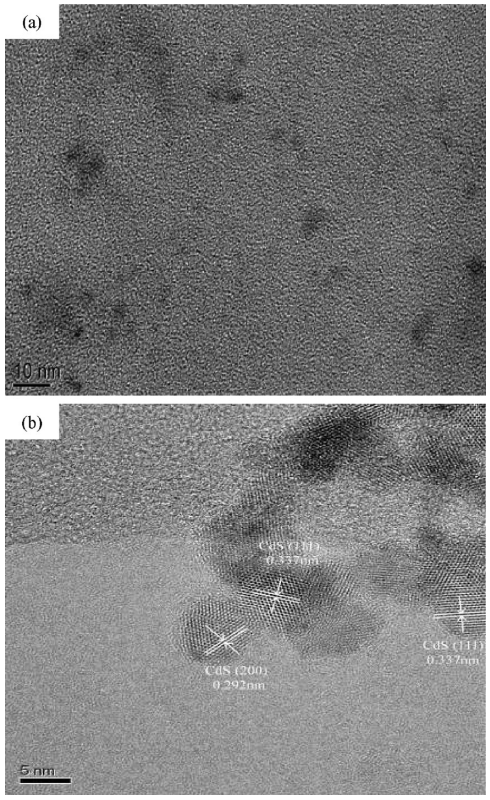

Figure 2. TEM and HRTEM micrographs of CdS QDs: (a) TEM and (b) HRTEM.

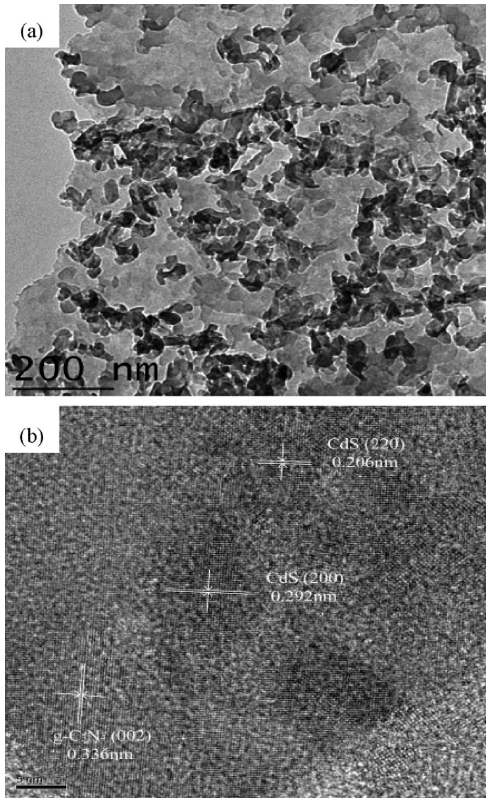

Figure 3. TEM and HR-TEM images of the samples. (a) TEM micrographs of CdS QDs/g-C_3N_4. (b) HR-TEM images of CdS QDs/g-C_3N_4 showing the arrangement of g-C_3N_4 and CdS crystallites.

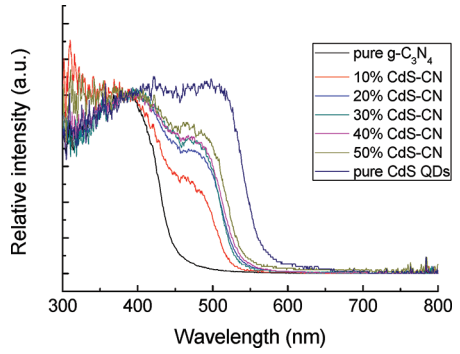

Figure 4. UV−vis diffuse absorption spectra of CdS QDs/g-C_3N_4 composite samples.

edge at 535 nm (10 wt % CdS/g-C_3N_4). CdS QDs/g-C_3N_4 composite samples show a slight shift of the g-C_3N_4 band gap and a shoulder on the adsorption edge that reaches further out in the visible region. These observations are attributed to the interaction between g-C_3N_4 and CdS QDs in the composite samples. The spectral range covered increases with the increase of the CdS QD content. The total absorption of the composite samples increases the production of electron−hole pairs. As a result, this may lead to a higher photocatalytic activity.

The chemical composition of the CdS QDs/g-C_3N_4 photocatalysts and the chemical state of the constituent elements were characterized by XPS (Figures 5 and 6). The

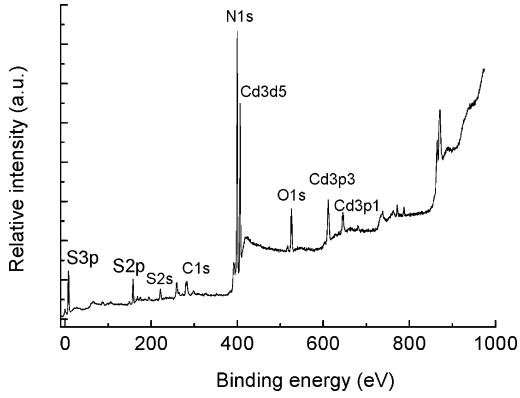

Figure 5. XPS survey spectrum of the 10 wt % CdS QDs/g-C_3N_4.

XPS results show that the sample contains the elements C, N, Cd, and S and a small amount of O. The photoelectron peaks appear at binding energies of 285 eV (C 1s), 400.1 eV (N 1s), 405 eV (Cd $3d_5$), and 162 eV (S 2p).

Figure 6a shows the C 1s XPS spectra of the 10 wt % CdS QDs/g-C_3N_4 composite sample: the C 1s peak can be deconvoluted into two peaks at ~285.1 and ~288.2 eV. The former peak is assigned to carbon atoms in a purely carbonaceous environment, that is, graphitic or amorphous carbons adsorbed on the surface.[25,39] In contrast, the latter peak originates from carbon atoms bonded to three nitrogen atoms in the g-C_3N_4 lattice.[40,41] The N 1s XPS spectra (Figure 6b) shows an asymmetrical feature indicating the coexistence of a number of nitrogen environments; fitting with three Gaussians results in binding energies of 398.8, 400.0, and 401.3 eV.[25] Two peaks at 400.0 and 401.3 eV can be assigned to tertiary nitrogen $(N-(C)_3)$ and amino functional groups having a hydrogen atom (C−N−H).[25,40] The peak at 398.8 eV is typically

dx.doi.org/10.1021/jp3041692 | J. Phys. Chem. C 2012, 116, 13708−13714

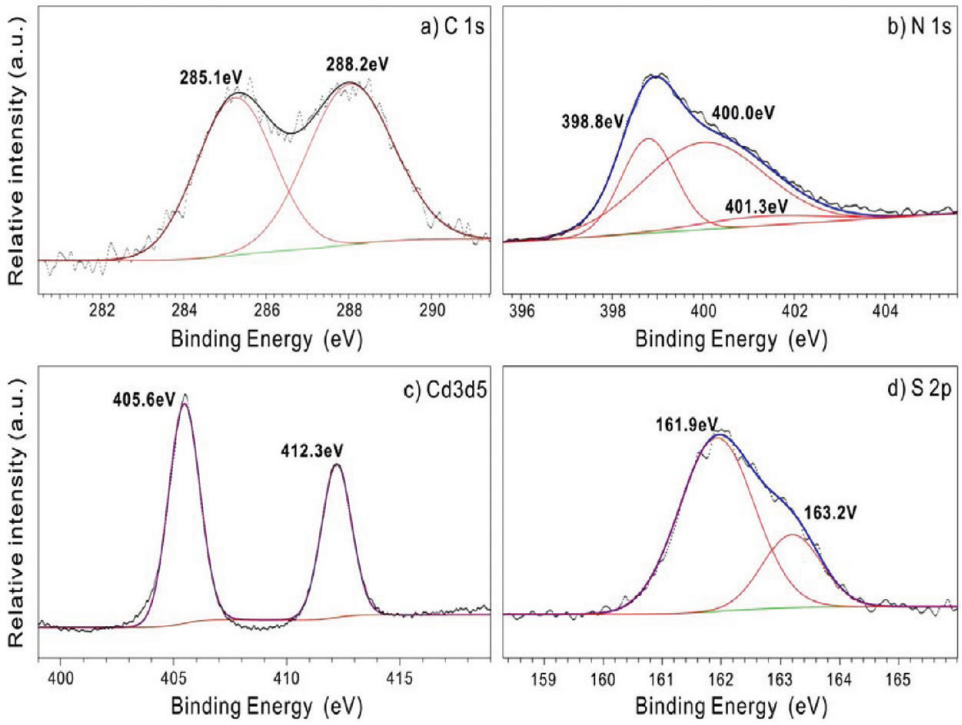

Figure 6. High-resolution XPS spectra of C 1s for the 10 wt % CdS QDs/g-C_3N_4: (a) C 1s; (b) N 1s; (c) Cd $3d_5$; (d) S 2p.

attributed to N atoms sp^2-bonded to two carbon atoms (C═N−C),[39,42] thus confirming the presence of sp^2-bonded graphitic carbon nitride. The photoelectron peaks for Cd $3d_5$ were observed at 405.6 and 412.3 eV (Figure 6c), which can be assigned to the Cd^{2+} ions of the CdS QDs.[40] Figure 6d shows the S 2p peak at 161.9 eV, as expected for the sulfide in CdS QDs.[43] In combination, Figure 6c,d confirms the presence of CdS QDs in the g-C_3N_4 photocatalyst.

The interaction of the CdS QDs with the g-C_3N_4 support was studied by FTIR spectroscopy. Figure 7 shows a comparison of FT-IR spectra of pure g-C_3N_4, pure CdS QDs, and the 30 wt % CdS QDs/g-C_3N_4 composite. In the first case, characteristic bands in the 1200−1700 cm^{-1} region dominate the spectrum, with peaks appearing at 1235, 1322, 1423, 1572, and 1640 cm^{-1}. These can be assigned to the stretching modes of CN heterocycles.[22,25] Additionally, the characteristic breathing mode of triazine units at 806 cm^{-1} is observed.[22] For pure CdS QDs, the broad and weak band around 664 cm^{-1} and the peaks between 1050 and 1660 cm^{-1} can be attributed to the Cd−S bond, with the exception of the band around 1630 cm^{-1}, which is the O−H bending vibration.[44,45] The peak at 1390 cm^{-1} can be attributed to the C−S band in the capping agent thioglycollic acid.[42] In the case of the CdS QDs/g-C_3N_4 composite, the bands for both g-C_3N_4 and CdS QDs appear, corroborating the formation of a composite photocatalysts. In addition, broad bands in the 3000−3800 and 2360 cm^{-1} regions can be observed for all samples, which correspond to physisorbed H_2O and CO_2 from the atmosphere, respectively.[46]

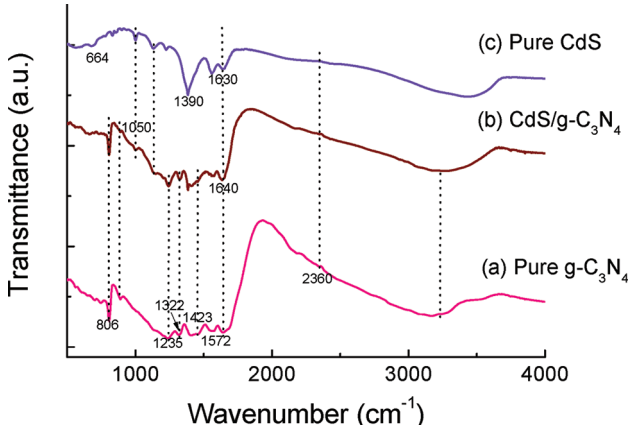

Figure 7. FT-IR spectra of the as-prepared samples: (a) pure g-C_3N_4; (b) 30 wt % CdS QDs/g-C_3N_4; (c) pure CdS.

3.2. Photocatalytic H_2 Production. Photocatalytic hydrogen evolution over different CdS QDs/g-C_3N_4 samples loaded with 1.0 wt % Pt was evaluated under visible light irradiation (>400 nm) using methanol as a scavenger to consume photoinduced holes. The cocatalyst Pt is intended to reduce the overpotential required for H_2 evolution from water. Control experiments indicated that no hydrogen evolution is observed in the absence of either light irradiation or photocatalyst. Figure 8 shows the H_2 evolution rate over the samples with different CdS QD loadings under visible light irradiation.

A significant impact of the CdS QD content is found: pure g-C_3N_4 samples evolve H_2 at a rate of 1.89 $\mu mol \cdot h^{-1}$ under visible light irradiation. Impregnation with CdS QDs improves the evolution rate up to a loading of 30 wt % where the highest H_2 photogeneration rate was found at 17.27 $\mu mol \cdot h^{-1}$. This is about 9.1 times higher than that of pure g-C_3N_4. It also exceeds the H_2 evolution rate of a pure CdS QD sample of 7.83 $\mu mol \cdot h^{-1}$ under the same irradiating conditions. Figure 8 emphasizes that the CdS QD content is pivotal for optimal photocatalytic activity: when the CdS QD content is increased beyond 30 wt %, a decrease in the photocatalytic H_2 evolution results. The origin of this effect can be explained as follows: the suitable CdS QD content causes their good dispersion on the g-

dx.doi.org/10.1021/jp3041692 | J. Phys. Chem. C 2012, 116, 13708−13714

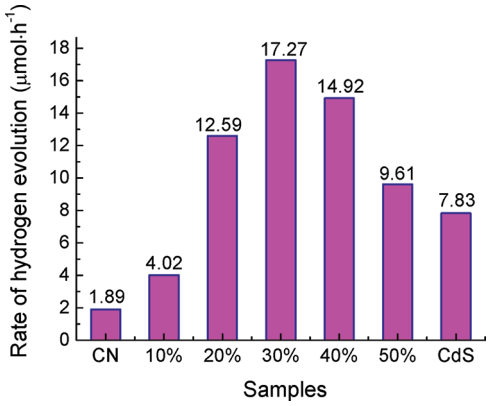

Figure 8. Comparison of the photocatalytic activity of the CdS QDs/g-C_3N_4 composite samples for the H_2 production from methanol aqueous solution under visible light irradiation (λ > 400 nm).

C_3N_4 surface, which favors the transfer and separation of the charge carriers. At a higher CdS QD content, the nanoclusters of CdS QDs species would have covered the surface of g-C_3N_4, reducing the density of g-C_3N_4 active sites available for H_2 evolution. A similar observation has been reported for CdS/TiO_2 composites.[34]

The transient photocurrent responses of 30 wt % CdS QDs/g-C_3N_4, of CdS QDs and of pure g-C_3N_4 samples were investigated for several on−off cycles of irradiation. Figure 9

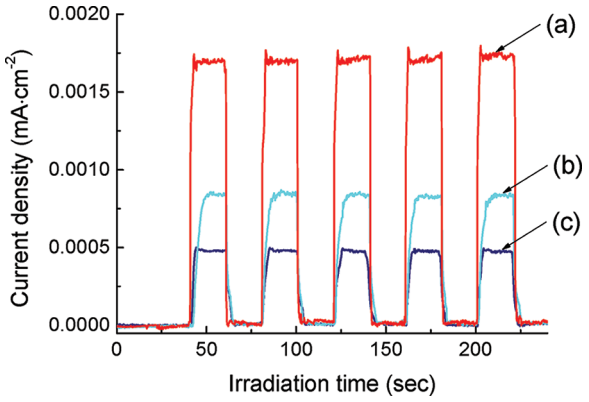

Figure 9. Transient photocurrent response for the (a) 30 wt % CdS QDs/g-C_3N_4, (b) CdS QDs, and (c) pure g-C_3N_4 samples. All the electrodes were evaluated in 0.01 M Na_2SO_4 aqueous solution under visible light irradiation using Ag/AgCl as reference electrode.

shows a plot of photocurrent density transients for as-prepared samples as the irradiation was switched on and off. The photocurrent values rapidly decrease to zero at the end of irradiation, underlining the photoactivated nature of the process. The CdS QDs/g-C_3N_4 composite photocatalyst shows the highest photocurrent intensity of the three samples, whereas the lowest photocurrent intensity can be found on the pure g-C_3N_4 sample. Besides activity, the stability of a photocatalyst is important for its application. To demonstrate the stability of our composite catalysts, we cycled the hydrogen evolution for 30 wt % samples. Figure 10 displays the H_2 evolution curve in a cycling photocatalytic run. No obvious decrease of H_2 evolution is observed after irradiation for 28 h. XRD analysis of the material before and after the experiment (Figure 11) also illustrates that the crystal structure has not changed; no photocorrosion is detected in the running period.

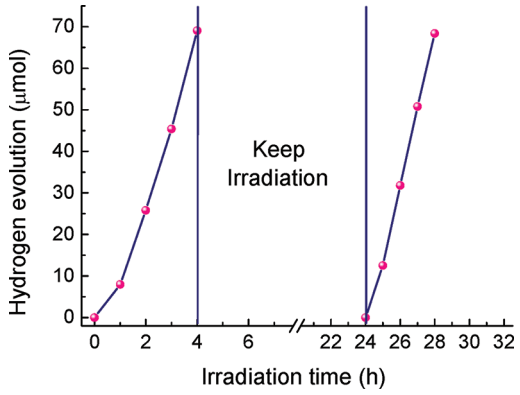

Figure 10. Cycling runs for the photocatalytic H_2 evolution in the presence of 30 wt % CdS QDs/g-C_3N_4 composite under visible light irradiation.

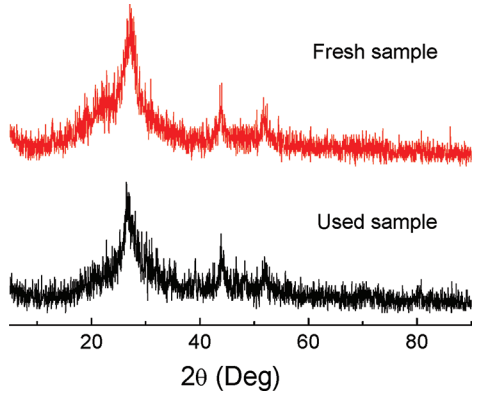

Figure 11. XRD patterns of as-prepared 30 wt % CdS QDs/g-C_3N_4 and the sample after it was used in cycling photocatalytic experiments.

3.3. Discussion of the Photocatalytic Mechanism. Both imaging of our composite (Figure 3) and the UV−vis absorption spectroscopy indicate a high dispersion of the CdS QDs in the g-C_3N_4 and their close contact, setting the stage for rapid charge transfer between the components of the composite. We investigated this transfer by photoluminescence measurements. Figure 12 presents the photoluminescence spectra for pure g-C_3N_4 and the QD-coupled CdS/C_3N_4 sample (30 wt % CdS content) at an excitation wavelength of 325 nm. The main emission peak is centered at about 459

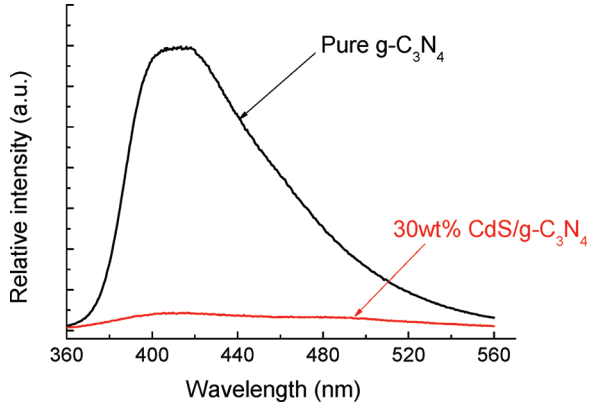

Figure 12. Comparison of photoluminescence (PL) spectra of pure g-C_3N_4 and CdS QDs/g-C_3N_4 samples.

dx.doi.org/10.1021/jp3041692 | J. Phys. Chem. C 2012, 116, 13708−13714

nm for the pure g-C_3N_4 sample, which can be attributed to recombination of electron−hole pairs in the g-C_3N_4.[42] Once CdS QDs are added, the photoluminescence drops markedly. We interpret the reduction of total photoluminescence yield as an indication of the efficient transfer of photoexcited holes and/or electrons between g-C_3N_4 and CdS QDs, which have a much smaller native luminescence. The samples used for PL experiments did not contain Pt as cocatalyst.

Our observation of increased photocatalytic hydrogen evolution activity of the composite compared to its pure components suggests separation of photogenerated electron−hole pairs to its components, so that their distance prevents efficient recombination and provides for longer lifetimes (Figure 13). The optimal loading at 30 wt % indicates the

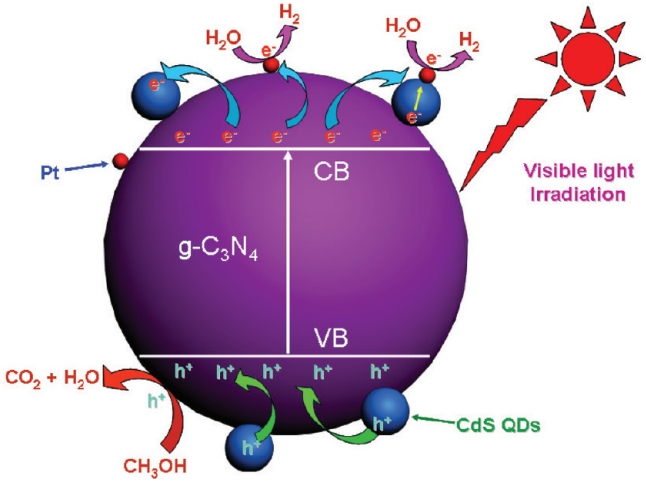

Figure 13. Schematic of photogenerated charge transfer in the CdS QDs/g-C_3N_4 system under visible light irradiation.

optimal balance between absorption in the g-C_3N_4 and transfer of the charge carriers to the CdS QDs. The photogenerated charge transfer in the CdS QDs/g-C_3N_4 composites is proposed and illustrated in Figure 13. The photogenerated electrons in g-C_3N_4 are transferred to CdS QDs due to the difference of CB edge potentials. The electrons then transferred from g-C_3N_4, and the electrons excited from the VB of CdS QDs will accumulate on the Pt nanoparticles and then participate in H_2 evolution. For the CdS QDs, the quantum size effect can increase the band gap of bulk CdS. The VB of CdS QDs may be lower than that of g-C_3N_4 due to the quantum size effect. The photogenerated holes on the VB of CdS QDs can migrate to that of g-C_3N_4. Therefore, both the efficient electron−hole separation and the excited electrons from CdS QDs lead to a significant enhancement of photocatalytic H_2 evolution in the CdS QDs/g-C_3N_4 composite system. The shift of the UV−vis absorption edges (Figure 4) with CdS QD loading may indicate that other effects contribute here also, which are beyond the characterization techniques available in our lab.

4. CONCLUSIONS

In summary, a series of CdS quantum dot-coupled graphitic carbon nitride (g-C_3N_4) photocatalysts with high visible light photocatalytic H_2 evolution activity were synthesized via a chemical impregnation method. It was shown that the CdS QDs/g-C_3N_4 composite had a red shift and strong absorption in the visible light region. After introduction of CdS QDs, the g-C_3N_4 showed efficient separation of the photogenerated charge carriers and enhancement of the visible light photocatalytic H_2 evolution activity. The optimal CdS QD content was found to be 30 wt %, and the corresponding H_2 evolution rate was 17.27 μmol·h^{-1}, which was about 9 times higher than that of pure g-C_3N_4. The synergic effect was explained based on PL spectra and photoelectrochemical measurements. The novel CdS QDs/g-C_3N_4 composite material, as highly efficient photocatalysts, can be a very promising candidate for the high-performance H_2 evolution photocatalysts.

AUTHOR INFORMATION

Corresponding Author

*E-mail: pingyun.feng@ucr.edu.

Notes

The authors declare no competing financial interest.

ACKNOWLEDGMENTS

This work was financially supported by the NSF (DMR-0907175 and CHE-1213795), the National Science Foundation of China (Grant No. 21003157), Beijing Nova Program (Grant No. 2008B76), and Science Foundation of China University of Petroleum, Beijing (Grant No. KYJJ2012-06-20). L.B. acknowledges support by the U.S. Department of Energy grant DE-FG02-07ER15842.

REFERENCES

(1) Chen, X. B.; Shen, S. H.; Guo, L. J.; Mao, A. S. *Chem. Rev.* **2010**, *110*, 6503−6570.
(2) Kudo, A.; Miseki, Y. *Chem. Soc. Rev.* **2009**, *38*, 253−278.
(3) Kudo, A. *MRS Bull.* **2011**, *36*, 32−38.
(4) Iwase, A.; Ng, Y. H.; Ishiguro, Y.; Kudo, A.; Amal, R. *J. Am. Chem. Soc.* **2011**, *133*, 11054−11057.
(5) Ouyang, S. X.; Ye, J. H. *J. Am. Chem. Soc.* **2011**, *133*, 7757−7763.
(6) Lv, J.; Kako, T.; Li, Z.; Zou, Z.; Ye, J. H. *J. Phys. Chem. C* **2010**, *114*, 6157−6162.
(7) Silva, L. A.; Ryu, S. Y.; Choi, J.; Choi, W.; Hoffmann, M. R. *J. Phys. Chem. C* **2008**, *112*, 12069−12073.
(8) Ge, L.; Xu, M. X.; Fang, H. B. *Appl. Surf. Sci.* **2006**, *253*, 2257−2263.
(9) Zong, X.; Wu, G.; Yan, H.; Ma, G.; Shi, J.; Wen, F.; Wang, L.; Li, C. *J. Phys. Chem. C* **2010**, *114*, 1963−1968.
(10) Ke, D.; Liu, S.; Dai, K.; Zhou, J.; Zhang, L.; Peng, T. *J. Phys. Chem. C* **2009**, *113*, 16021−16026.
(11) Zuo., F.; Wang, L.; Wu, T.; Zhang, Z. Y.; Borchardt, D.; Feng, P. Y. *J. Am. Chem. Soc.* **2010**, *132*, 11856−11857.
(12) Wang, D.; Zou, Z.; Ye, J. *Catal. Today* **2004**, *93*−*95*, 891−894.
(13) Wang, D.; Tang, J.; Zou, Z.; Ye, J. *Chem. Mater.* **2005**, *17*, 5177−5182.
(14) Yin, J.; Zou, Z.; Ye, J. *Chem. Phys. Lett.* **2003**, *378*, 24−28.
(15) Liu, M.; You, W.; Lei, Z.; Takata, T.; Domen, K.; Li, C. *Chin. J. Catal.* **2006**, *27*, 556−558.
(16) Yamasita, D.; Takata, T.; Hara, M.; Kondo, J. N.; Domen, K. *Solid State Ionics* **2004**, *172*, 591−595.
(17) Zhang, Z. Y.; Lin, Q. P.; Zheng, S. T.; Bu, X. H.; Feng, P. Y. *Chem. Commun.* **2011**, *47*, 3918−3920.
(18) Wang, X.; Maeda, K.; Thomas, A.; Takanabe, K.; Xin, G.; Carlsson, J. M.; Domen, K.; Antonietti, M. *Nat. Mater.* **2008**, *8*, 76−80.
(19) Liu, G.; Niu, P.; Sun, C.; Smith, S. C.; Chen, Z.; Lu, G. Q.; Cheng, H. M. *J. Am. Chem. Soc.* **2010**, *132*, 11642−11648.
(20) Zhang, J.; Chen, X.; Takanabe, K.; Maeda, K.; Domen, K.; Epping, J. D.; Fu, X.; Antonietti, M.; Wang, X. *Angew. Chem., Int. Ed.* **2010**, *49*, 441−444.
(21) Su, F. Z.; Mathew, S. C.; Lipner, G.; Fu, X. Z.; Antonietti, M. *J. Am. Chem. Soc.* **2010**, *132*, 16299−16301.

(22) Yan, S. C.; Li, Z. S.; Zou, Z. G. *Langmuir* **2009**, *25*, 10397−10401.
(23) Zhang, Y. J.; Mori, T.; Ye, J. H.; Antonietti, M. *J. Am. Chem. Soc.* **2010**, *132*, 6294−6295.
(24) Chen, X. F.; Zhang, J. S.; Fu, X. Z.; Antonietti, M.; Wang, X. C. *J. Am. Chem. Soc.* **2009**, *131*, 11658−11659.
(25) Xiang, Q. J.; Yu, J. G.; Jaroniec, M. *J. Phys. Chem. C* **2011**, *115*, 7355−7363.
(26) Zhang, Y. J.; Mori, T.; Niu, L.; Ye, J. H. *Energy Environ. Sci.* **2011**, *4*, 4517−4521.
(27) Zhang, Y. J.; Thomas, A.; Antonietti, M.; Wang, X. C. *J. Am. Chem. Soc.* **2009**, *131*, 50−51.
(28) Yan, H. J.; Huang, Y. *Chem. Commun.* **2011**, *47*, 4168−4170.
(29) Robel, I.; Subramanian, V.; Kuno, M.; Kamat, P. V. *J. Am. Chem. Soc.* **2006**, *128*, 2385−2393.
(30) Lee, Y. L.; Huang, B. M.; Chien, H. T. *Chem. Mater.* **2008**, *20*, 6903−6905.
(31) Gao, X. F.; Li, H. B.; Sun, W. T.; Chen, Q.; Tang, F. Q.; Peng, L. M. *J. Phys. Chem. C* **2009**, *113*, 7531−7535.
(32) Sambur, J. B.; Novet, T.; Parkinson1, B. A. *Science* **2010**, *330*, 63−66.
(33) Li, T. L.; Teng, H. *J. Mater. Chem.* **2010**, *20*, 3656−3664.
(34) Sun, W. T.; Yu, Y.; Pan, H. Y.; Gao, X. F.; Chen, Q.; Peng, L. M. *J. Am. Chem. Soc.* **2008**, *130*, 1124−1125.
(35) Gao, X. F.; Sun, W. T.; Hu, Z. D.; Ai, G.; Zhang, Y. L.; Feng, S.; Li, F.; Peng, L. M. *J. Phys. Chem. C* **2009**, *113*, 20481−20485.
(36) Daskalaki, V.; A ntoniadou, M.; Lipuma, G.; Kondarides, D.; Lianos, P. *Environ. Sci. Technol.* **2010**, *44*, 7200−7205.
(37) Ge, L. *Mater. Lett.* **2011**, *65*, 2652−2654.
(38) Ge, L.; Liu, J. *Appl. Catal., B* **2011**, *105*, 289−297.
(39) Yan, S. C.; Li, Z. S.; Zou, Z. G. *Langmuir* **2010**, *26*, 3894−3901.
(40) Thomas, A.; Fischer, A.; Goettmann, F.; Antonietti, M.; Muller, J.; Schlogl, R.; Carlsson, J. M. *J. Mater. Chem.* **2008**, *18*, 4893−4908.
(41) Khabashesku, V. N.; Zimmerman, J. L.; Margrave, J. L. *Chem. Mater.* **2000**, *12*, 3264−3270.
(42) Li, X. F.; Zhang, J.; Shen, L. H.; Ma, Y. M.; Lei, W. W.; Cui, Q. L.; Zou, G. T. *Appl. Phys. A: Mater. Sci. Process.* **2009**, *94*, 387−392.
(43) Crist, B. V. *Handbook of the Elements and Native Oxides*; XPS International, Inc.: Mountain View, CA, 1999.
(44) Sobhana, S. S. L.; Vimala, D. M.; Sastry, T. P.; Mandal, A. B. *J. Nanopart. Res.* **2011**, *13*, 1747−1757.
(45) Tang, S. H.; Li, Y. Q. *J. Colloid Interface Sci.* **2011**, *360*, 71−77.
(46) Liu, S. W.; Yu, J. G.; Wang, W. G. *Phys. Chem. Chem. Phys.* **2010**, *12*, 12308−12315.